Cite this article
Bergami AV, Pelle A, Fiorentino G *et al.*
Seismic assessment of corroded concrete bridges using incremental modal pushover analysis.
Proceedings of the Institution of Civil Engineers – Bridge Engineering,
https://doi.org/10.1680/jbren.21.00025

Research Article
Paper 2100025
Received 14/06/2021;
Accepted 21/09/2021

Bridge Engineering

ice Publishing

Seismic assessment of corroded concrete bridges using incremental modal pushover analysis

Alessandro Vittorio Bergami
Q1 Assistant Professor, Department of Architecture, Roma Tre University, Rome, Italy (Orcid:0000-0002-7761-2190) (corresponding author: alessandro.bergami@uniroma3.it)

Angelo Pelle
PhD student, Department of Architecture, Roma Tre University, Rome, Italy (Orcid:0000-0001-5842-7531)

Gabriele Fiorentino
Marie Curie Research Fellow, Department of Civil Engineering, University of Bristol, Bristol, UK (Orcid:0000-0002-6444-0473)

Davide Lavorato
Professor, Department of Architecture, Roma Tre University, Rome, Italy (Orcid:0000-0001-7753-1975)

Gian Felice Giaccu
Assistant Professor, Department of Architecture, Design and Urban Planning, University of Sassari, Alghero, Italy (Orcid:0000-0002-7227-6618)

Giuseppe Quaranta
Professor, Department of Structural and Geotechnical Engineering, Sapienza University of Rome, Rome, Italy (Orcid:0000-0001-8295-0912)

Bruno Briseghella
Full Professor, College of Civil Engineering, Fuzhou University, University Town, Fuzhou, Fujian, PR China (Orcid:0000-0002-8002-2298)

Camillo Nuti
Full Professor, Department of Architecture, Roma Tre University, Rome, Italy (Orcid:0000-0002-0385-201X)

An efficient yet accurate procedure was developed for the seismic assessment of reinforced concrete (RC) bridges subject to chloride-induced corrosion. The procedure involves using incremental modal pushover analysis to assess corroded bridges as an alternative and less computationally demanding approach to non-linear dynamic analysis. A multi-physics finite-element analysis is performed to evaluate the effects of chloride-induced corrosion on bridge columns. In doing so, chloride ingress in concrete is numerically simulated as a diffusion process by considering the effects of temperature, humidity, corrosion-induced cover cracking and concrete aging. The estimated chloride concentration is then employed to evaluate the corrosion current density, from which the effects of corrosion on reinforcement, cracked cover concrete, confinement and plastic hinge length can be determined for subsequent non-linear static analysis. A case study of a typical bridge structure is presented. The proposed procedure can be used to assess the seismic performance of irregular RC bridges exposed to severe corrosive environments.

Keywords: bridges/concrete structures/corrosion

Q2 Notation

A_s	area of uncorroded reinforcing steel bar
A_s'	area of corroded reinforcing steel bar
b	hardening ratio
C_{bc}	concentration of bound chlorides
C_{fc}	concentration of chlorides dissolved in pore solution (free chlorides)
C_{tc}	total chloride concentration
c	concrete cover thickness
D_c^*	apparent diffusion coefficient
$D_{c,ref}$	reference chloride diffusion coefficient
D_h	humidity diffusion coefficient
$D_{h,ref}$	reference humidity diffusion coefficient
E	elastic modulus
$F_h(h)$	corrective factor of chloride diffusion coefficient taking into account the effect of pore relative humidity
$F_t(t)$	corrective factor of chloride diffusion coefficient taking into account the effect of concrete age
$F_\delta(\delta)$	corrective factor of chloride diffusion coefficient taking into account the effect of cover crack width
$F_\tau(\tau)$	corrective factor of chloride diffusion coefficient taking into account the effect of temperature
f_{rn-1}	skeleton curve: steel yielding stress (inversion)
f_{yn}	skeleton curve: steel yielding stress
h	pore relative humidity
i_{corr}	corrosion current density
M	bending moment
$P_{i,IMPA\beta}$	performance point for seismic intensity level i
p	pit depth
q	design behaviour factor
R	pitting factor
R_c	ohmic resistance of concrete
R_G	gas constant
R_s	parameter governing the transition from the elastic to the inelastic branch
S_a	elastic acceleration spectral value
T	period
t	concrete age
t_e	equivalent hydration age
t_{ref}	reference exposure time
U_c	activation energy of chloride diffusion process

u_r	deck displacement in transverse direction
$u_{r,i,MPA}$	deck displacement obtained for *i*th intensity level from modal pushover analysis (MPA)
$u_{r,i,UPA}$	deck displacement obtained for *i*th intensity level from uniform pushover analysis (UPA)
u_u	ultimate displacement
u_y	yielding displacement
V_b	base shear
$V_{b,i,MPA}$	base shear obtained for *i*th intensity level from MPA
$V_{b,i,UPA}$	base shear obtained for *i*th intensity level from UPA
α_L, β_L	binding isotherm constants
δ	concrete crack width
Q3 ε'	corroded ultimate strain of reinforcing steel bar
ε_1'	average tensile strain of cracked concrete
ε_c	strain at peak concrete compressive strength
ε_{rm-1}	skeleton curve: steel yielding strain (inversion)
ε_{su}	uncorroded ultimate strain of reinforcing steel bar
ε_{yn}	skeleton curve: steel yielding strain
μ	age factor
τ	temperature
τ_{ref}	constant reference temperature
χ	curvature
ψ	mass loss ratio of corroded rebar
ω_e	water held in capillary and gel pores

1. Introduction

The assessment of reinforced concrete (RC) bridges exposed to chlorides deserve careful investigation since dramatic and rapid corrosion of the reinforcing steel bars can occur under these conditions. In this regard, the analysis of corroded RC bridges is especially relevant in earthquake-prone areas where severe corrosion phenomena induced by chlorides might compromise their proper seismic response.

Within this framework, Alipour *et al.* (2011, 2013) presented a comprehensive numerical framework for the seismic assessment of RC bridges under chloride-induced corrosion. A multi-physics simulation of chloride ingress was performed by assuming that the process is dominated by the diffusion phenomenon under the simultaneous influence of environmental conditions (i.e. temperature and humidity) and concrete aging. Non-linear structural analyses were presented for multi-span regular RC bridges whose deck section consisted of box girders. The deck was modelled using linear-elastic elements while the columns were modelled using inelastic beam–column elements, where the plasticity was concentrated over a specified length of the element ends. Non-linear dynamic analyses were performed by Alipour *et al.* (2011) to evaluate the temporal evolution of the deck drift ratio. The moment–curvature response of the bridge columns was discussed by Alipour *et al.* (2013), together with the results of standard non-linear static (pushover) analyses.

A more recent study on the residual capacity of RC bridges under chloride-induced corrosion was reported by Zhou *et al.* (2019). Therein, chloride ingress was simulated as a diffusion process and the multi-physics analysis accounted only for the influence of the temperature. A reliability assessment of an existing RC arch bridge under static load was considered as a case study.

Another recent study on the capacity assessment of corroded bridges was conducted by Conti *et al.* (2020). In that study, chloride ingress was still simulated as a pure diffusion process, without considering the concurrent influence of other parameters. In particular, the residual capacity of RC grillage decks under static loads was investigated.

Non-linear models of corroded RC bridge columns with rectangular and circular cross-sections were examined by Dizaj and Kashani (2020) and Dizaj (2021) by taking into account Q4 inelastic buckling and low-cycle fatigue phenomena of corroded reinforcing steel bars. These studies did not include simulations of the corrosion process, but they do shed light on the sensitivity of failure mechanisms under corrosion. State-of the-art reviews about the capacity assessment of RC bridges under corrosion are available in the literature (Andisheh *et al.*, 2016; Kashani *et al.*, 2019).

With this background, a comprehensive yet simplified approach for the seismic assessment of corroded RC bridges exposed to chlorides is presented in this paper. The main motivation of this study was to develop a computational framework for the seismic assessment of corroded RC bridges that provides sufficiently accurate results while reducing the overall computational effort. In the proposed framework, the recent methodology of incremental modal pushover analysis (IMPA) is applied to reduce both the elaboration time and modelling effort required in seismic assessments of bridges as compared with incremental dynamic analysis (IDA). Multi-physics finite-element (FE) based simulations are then performed to estimate the chloride concentration in concrete.

As in previous studies, multi-physics analysis is performed, considering the effects of temperature, humidity and concrete aging. However, different from most previous studies on the seismic assessment of RC bridges, the effect of concrete cover cracking due to rebar corrosion is also considered by resorting to experimental relationships, once again to alleviate the overall elaboration time and modelling effort. The chloride concentration obtained from the multi-physics analysis is then used to quantify the effects of corrosion on reinforcing steel bars, cracked cover concrete, confinement and plastic hinge length for the next non-linear static analyses. Application of the proposed approach is illustrated with reference to

an irregular RC bridge with columns affected by severe pitting corrosion phenomena.

2. IMPA for RC bridges

IMPA is a non-linear static procedure originally developed for buildings (Bergami *et al.*, 2015) and then specialised for bridge structures (IMPAβ) (Bergami *et al.*, 2017, 2020a, 2020b). The method requires the parallel implementation of two pushover procedures – a pushover with a uniform load pattern (uniform pushover analysis (UPA)) and modal pushover analysis (MPA). Overall, IMPAβ is articulated in the following main steps (Figure 1).

- Estimation of the seismic capacity of the bridge by performing the two different pushover procedures, namely UPA and MPA (steps 1a and 1b in Figure 1).
- Definition of the seismic demand in terms of the response spectrum for a given range of seismic intensity levels (step 1c in Figure 1).
- Evaluation of the performance point (PP) within the predefined range of seismic intensity levels by means of both pushover procedures. Note that the MPA requires the combination of the results carried out from each modal shape to obtain a multi-modal PP (step 2 in Figure 1).
- The PP for seismic intensity level i is given by (step 3 in Figure 1

$$P_{i,\mathrm{IMPA}\beta} = [\max(u_{\mathrm{r},i,\mathrm{MPA}},\ u_{\mathrm{r},i,\mathrm{UPA}}),\ \max(V_{\mathrm{b},i,\mathrm{MPA}},\ V_{\mathrm{b},i,\mathrm{UPA}})] \quad (1)$$

where $(u_{\mathrm{r},i,\mathrm{UPA}},\ V_{\mathrm{b},i,\mathrm{UPA}})$ and $(u_{\mathrm{r},i,\mathrm{MPA}},\ V_{\mathrm{b},i,\mathrm{MPA}})$ are the coordinates of the PP for the ith intensity level as obtained by means of UPA and MPA, respectively. Herein, $u_{\mathrm{r},i,\mathrm{UPA}}$ and $V_{\mathrm{b},i,\mathrm{UPA}}$ are the deck displacement and base shear obtained for the ith intensity level from UPA, respectively, whereas $u_{\mathrm{r},i,\mathrm{MPA}}$ and $V_{\mathrm{b},i,\mathrm{MPA}}$ are the corresponding values calculated by means of MPA.
- Description of the structural response either in terms of deck displacement (u_{r}) and base shear (V_{b}) or in terms of u_{r} (here intended as damage measure) and seismic intensity such as peak ground acceleration (PGA) (step 4 in Figure 1). The deck displacement is tracked with reference to a representative node of the bridge (also known as a monitoring point).

3. Multi-physics analysis of RC bridges exposed to chlorides

3.1 Analysis of chloride ingress into concrete

In agreement with previous studies (Alipour *et al.*, 2011, 2013; Kwon *et al.*, 2009; Shafei *et al.*, 2012, 2013; Zhou *et al.*, 2019),

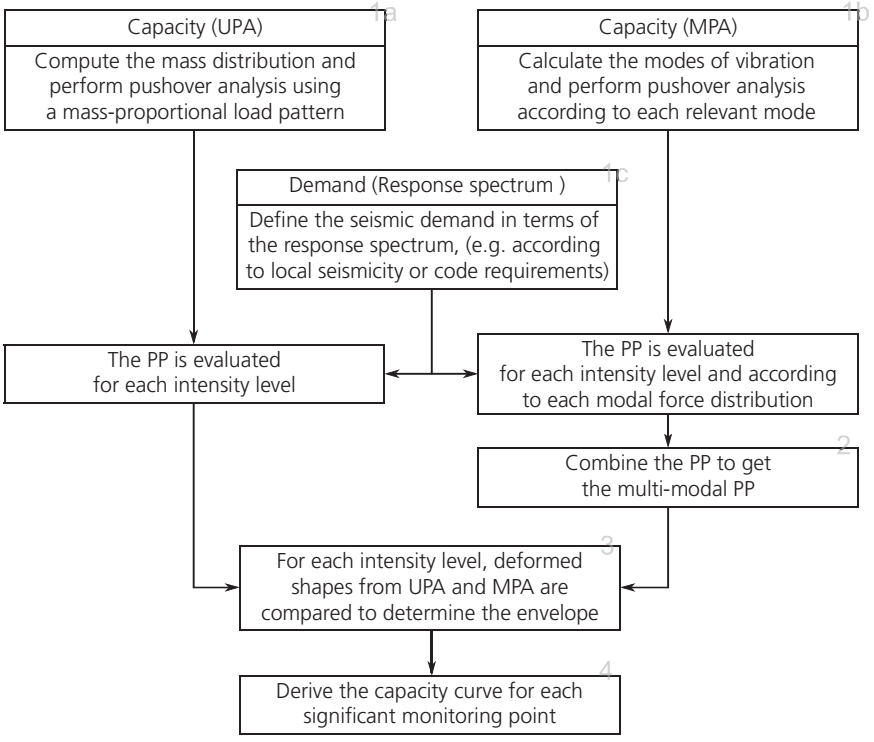

Figure 1. Flowchart of IMPAβ

it is assumed that chloride ingress into concrete can be approximated as a diffusion process. Conversely, it is presumed that chlorides cannot pass through the reinforcing steel bars. For the sake of conciseness, only the most important aspects of the numerical modelling of chloride ingress are given here. More details about the models and numerical values of the involved parameters are provided elsewhere (e.g. Alipour *et al.*, 2011, 2013; Kwon *et al.*, 2009; Shafei *et al.*, 2012, 2013; Zhou *et al.*, 2019). It is assumed that the bridge is made using ordinary Portland cement, with a cement content of 400 kg of cement per cubic metre of concrete and a water/cement ratio of 0.5.

Given the geometrical two-dimensional (2D) domain of a bridge member described by the set of coordinates (x, y) and introducing the time variable t (s), Fick's second law (for isotropic diffusion conditions) can be formalised as:

$$2. \quad \frac{\partial C_{fc}}{\partial t} = \frac{\partial}{\partial x}\left(D_c^* \frac{\delta C_{fc}}{\delta x}\right) + \frac{\partial}{\partial y}\left(D_c^* \frac{\partial C_{fc}}{\partial y}\right)$$

where C_{fc} (kg/m^3 of pore solution) is the concentration of chlorides dissolved in the pore solution (free chlorides), which is related to the total chloride concentration C_{tc} (kg/m^3 of concrete) through the relationship:

$$3. \quad C_{tc} = C_{bc} + \omega_e C_{fc}$$

where C_{bc} (kg/m^3 of concrete) is the concentration of bound chlorides and ω_e (m^3 of evaporable water/m^3 of concrete) is the water held in both capillary and gel pores. D_c^* (m^2/s) is the apparent diffusion coefficient, given by:

$$4. \quad D_c^* = \frac{D_c}{1 + (1/\omega_e)(\partial C_{bc}/\partial C_{fc})}$$

where $\partial C_{bc}/\partial C_{fc}$ is also known as the binding capacity and D_c is defined in Equation 6.In the present work, the Langmuir isotherm was employed, from which it is found that: Q6

$$5. \quad C_{bc} = \frac{\alpha_L C_{fc}}{1 + \beta_L C_{fc}} \rightarrow \frac{\partial C_{fc}}{\partial C_{fc}} = \frac{\alpha_L}{(1 + \beta_L C_{fc})^2}$$

where α_L (m^3 of pore solution/m^3 of concrete) and β_L (m^3 of pore solution/kg) are given constants. The Langmuir isotherm was here employed here, assuming $\alpha_L = 0.39$ m^3 of pore solution/m^3 of concrete and $\beta_L = 0.07$ m^3 of pore solution/kg.

Several physical, chemical and mechanical concurrent phenomena influence chloride diffusion. In the present work, D_c in Equation 4 was calculated as:

$$6. \quad D_c = D_{c,ref} F_\tau(\tau) F_h(h) F_\delta(\delta) + F_t(t)$$

where $D_{c,ref}$ (m^2/s) is the reference chloride diffusion coefficient; $D_{c,ref} = 4.5 \times 10^{-12}$ m^2/s is assumed. The functions $F_\tau(\tau)$, $F_h(h)$, $F_\delta(\delta)$ and $F_t(t)$ are corrective factors of the chloride diffusion coefficient that take into account the effects of temperature τ (K), pore relative humidity h, cover crack width δ (mm) and concrete age t (s), respectively.

In agreement with most existing studies, the dependence of chloride diffusivity on temperature is estimated using the Arrhenius law:

$$7. \quad F_\tau(\tau) = \exp\left[\frac{U_c}{R_G}\left(\frac{1}{\tau_{ref}} - \frac{1}{\tau}\right)\right]$$

where U_c (kJ/mol) is the activation energy of the chloride diffusion process ($U_c = 44.6$ kJ/mol), $R_G = 8.314 \times 10^{-3}$ kJ/(K.mol) is the gas constant and $\tau_{ref} = 296.15$ K is the constant reference temperature. Heat transfer in concrete and steel is modelled in a simplified way through Fourier's heat conduction law equation under isotropic conditions.

In the existing literature, it is also common to account for the effects of the pore relative humidity h through the corrective factor:

$$8. \quad F_h(h) = \left[1 + \left(\frac{1-h}{1-h_c}\right)^4\right]^{-1}$$

where h_c is the value of h at which D_c drops halfway between its highest and lowest value. The value of h_c is constant and equal to 0.75. In agreement with previous studies, moisture transport is modelled as a diffusion process. In doing so, the humidity diffusion coefficient D_h (m/s^2) is calculated as $D_h = D_{h,ref} G_\tau(\tau) G_h(h) G_{t_e}(t_e)$, where $D_{h,ref}$ (m^2/s) is the reference humidity diffusion coefficient. It is assumed that $D_{h,ref} = 2.00 \times 10_{-11}$ m^2/s. $G_\tau(\tau)$ and $G_h(h)$ are corrective factors that consider the effects due to temperature τ (K) and pore relative humidity h, respectively, whereas $G_{t_e}(t_e)$ accounts for the effects related to the equivalent hydration age t_e (days). Q7

Unlike most previous studies on the assessment of RC bridges subjected to chloride-induced corrosion, the effect of cover cracking due to the production of rust is also accounted for in the proposed model. To this end, in place of a time-consuming numerical simulation of the cracking process, experimental results are preferable in order to alleviate the overall computational burden. In fact, Fick's second law is often used to

estimate chloride penetration into concrete even when cracks are present and, in agreement with this assumption, several experimental studies have been performed to evaluate the corresponding amplification factor for the reference chloride diffusion coefficient as a function of the crack width δ (Kwon *et al.*, 2009; Zhang *et al.*, 2011). In the present study, the following experimental relationship (derived by Zhang *et al.* (2011)) was used to evaluate magnification of the chloride diffusion coefficient for a cracked concrete cover:

$$9. \quad F_\delta(\delta) = \max\{1,\ 47.18\delta^2 - 8.18\delta + 1\}$$

Equation 9 was applied up to the maximum crack width reported by Zhang *et al.* (2011) ($\delta_{max} = 0.5$ mm). Above this threshold, $F_\delta(\delta_{max})$ is assumed. This large amplification of the reference chloride diffusion coefficient is basically intended to simulate the acceleration of chloride penetration starting from the onset of cover spalling, which usually occurs at crack widths of about 1 mm (Pang *et al.*, 2020). The value of δ is determined according to the experimental relationship provided by Vidal *et al.* (2004) as a function of the loss of rebar cross-sectional area.

Finally, the effect of concrete age on the chloride diffusion coefficient is estimated as:

$$10. \quad F(t)_t = \left(\frac{t_{ref}}{t}\right)^{\mu}$$

where t_{ref} (s) is the reference exposure time and μ is the age factor. In this work, t_{ref} was considered to be 28 days and $\mu = 0.15$.

It might be useful to refer to Figure 2 for a quantitative assessment of the effects due to temperature (τ), pore humidity (h), crack width (δ) and concrete age (t) on chloride transport (here it is assumed $\omega_e = 0.15$ m^3 of evaporable water/m^3 of concrete and $C_{fc} = 10$ kg/m^3 of pore solution).

3.2 Effects of chloride-induced corrosion

The effects of chloride-induced corrosion are determined as a function of the corrosion current density i_{corr} (μA/cm^2). To this end, the experimentally calibrated relationship proposed by Liu and Weyers (1998) was adopted:

$$11. \quad \ln 1.08 i_{corr} = 7.89 + 0.7771 \ln 1.69 C_{tc} - \frac{3006}{\tau} - 0.000116 R_c + 2.24 t^{-0.215}$$

with t in years. In Equation 11, R_c is the ohmic resistance of concrete, which decreases as the amount of chlorides increases (Liu, 1996; Liu and Weyers, 1998).

It is presumed that the loss of rebar cross-section is dominated by pitting corrosion, which is simulated according to the model adopted by Val (2007). Overall, the increment of the pit

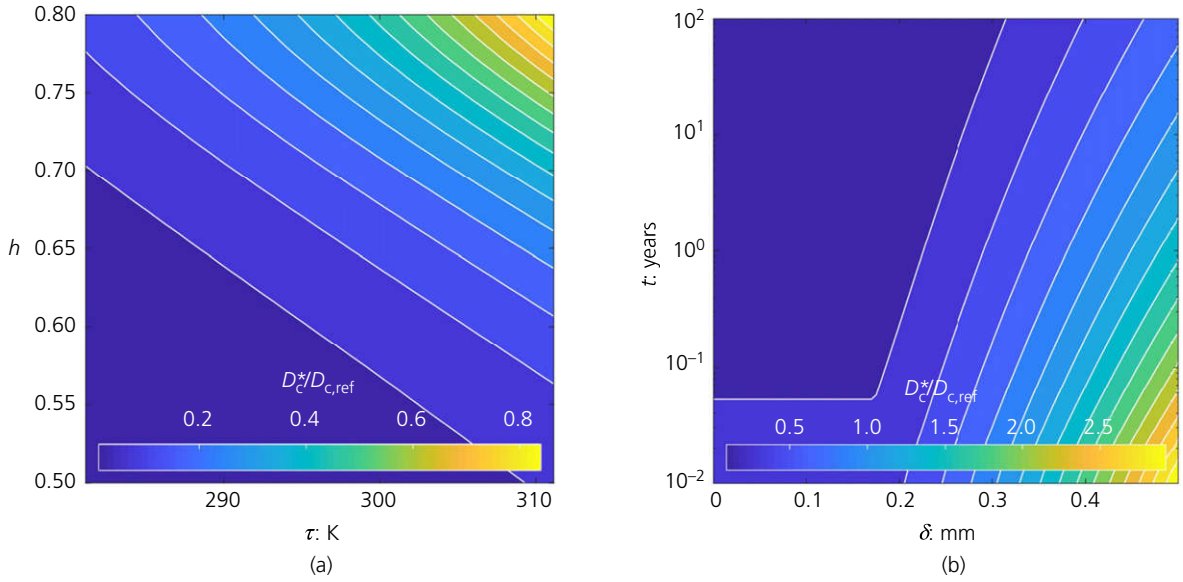

Figure 2. Ratio of current and reference chloride diffusion coefficient ($D_c^*/D_{c,ref}$) for sound concrete after 28 days: (a) as function of τ and h; (b) as a function of δ and t ($\tau = 296.15$ K and $h = 0.75$)

depth Δp (mm) is evaluated as follows:

12. $$\Delta p = 0.0116 i_{\text{corr}} \Delta t R$$

where Δt (years) is the time step and R is the pitting factor. At each time instant, the pit depth p (mm) is obtained as the cumulative sum of the corresponding previous increments. The area of the corroded reinforcing steel bar A_s' (mm2) at time t (years) is:

13. $$A_s^{'} = A_s - A_p$$

where A_s (mm^2) is the original (uncorroded) area of a reinforcing steel bar whose initial diameter is D_s. The loss of rebar cross-sectional area is calculated as follows and illustrated in Figure 3 (Val, 2007). Q8

14a.
$$\begin{aligned} A_p &= A_1 + A_2 && \text{if } p \le D_s/\sqrt{2} \\ A_p &= A_s - A_1 + A_2 && \text{if } D_s/\sqrt{2} < p \le D_s \\ A_p &= A_s && \text{if } p > D_s \end{aligned}$$

14b. $$A_1 = \frac{1}{2}\left[\theta_1 \left(\frac{D_s}{2}\right)^2 - a\left|\frac{D_s}{2} - \frac{p^2}{D_s}\right|\right]$$

14c. $$A_2 = \frac{1}{2}\left[\theta_2 p^2 - a\frac{p^2}{D_s}\right]$$

14d. $$A_2 = \frac{1}{2}\left[\theta_2 p^2 - a\frac{p^2}{D_s}\right]$$

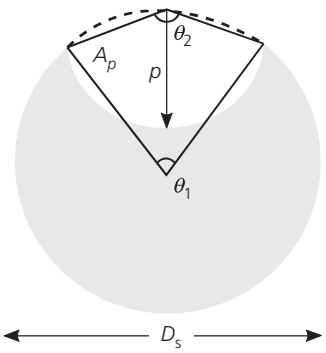

Figure 3. Geometry of pit in corroded rebar cross-section

14e. $$\theta_1 = 2\arcsin\frac{a}{D_s}$$

14f. $$\theta_2 = 2\arcsin\frac{a}{2p}$$

Apart from the large loss of rebar cross-section, pitting corrosion also strongly affects the ductility because, when the reinforcing steel bar is stretched by a tensile force, strain is concentrated in deeper notches. Thus, the overall elongation will be developed in small zones and, consequently, the average strain will be less at failure as compared with an uncorroded bar. To take into account the effect of strain concentration on the ultimate strain of corroded bars, the exponential decay law proposed by Imperatore *et al.* (2017) was employed. Moreover, the effects of concrete cover cracking and spalling due to rust production are also considered by reducing the strength of the cover concrete, as suggested by Coronelli and Gambarova (2004).

4. Numerical investigation

4.1 Case study

The considered bridge (Figure 4), designed in compliance with Eurocode 8 (BSI, 2011, 2013), has a straight deck and four equal spans (total length of 200 m). The deck is supported by piers (through unidirectional bearings at 50 m, 100 m and 150 m) in such a way that the corresponding transverse displacements are equal to each other whereas the longitudinal displacements are disconnected. A unidirectional bearing that restrains the transverse displacement of the deck was placed on the abutment at 0 m; on the other side (at 200 m) is a fixed bearing that restrains all displacements. C30/37 concrete and reinforcement with a characteristic yield strength of 450 MPa were used in the design. The overall aim of the analysis of this case study was to infer key aspects about the response of newly built irregular RC bridges exposed to a severe corrosive environment close to the Mediterranean coast. Q9

A behaviour factor $q = 3.0$ was used to evaluate the seismic action. The design response spectrum was defined according to the Italian technical code (MDIT, 2018) under the following assumptions: (*a*) the building site is in Reggio Calabria (a coastal city in southern Italy within a high seismic zone); (*b*) soil type B; (*c*) a return period of 949 years (life safety limit state). The static design loads are listed in Table 1.

The bridge has an irregular layout. The columns are of different heights and of circular cross-section (diameter of 2.5 m).

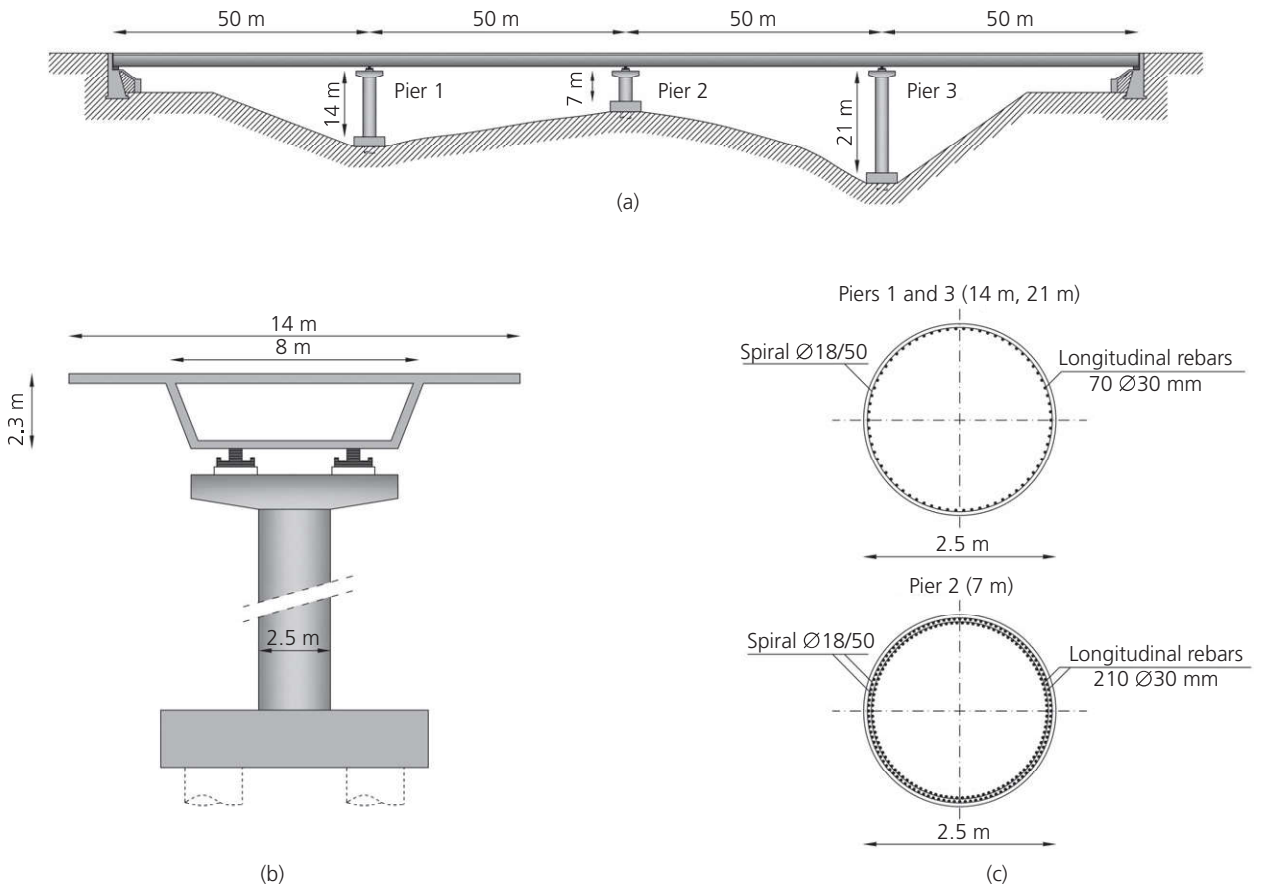

Figure 4. Layout of the considered RC bridge: (a) longitudinal view showing column heights and span lengths; (b) elevation view of generic bridge column; (c) cross-sections of bridge columns

The reinforcement of the columns is shown described in Figure 4(c). Two concrete cover values were considered.

- A concrete cover (c) of 50 mm was considered to evaluate the effectiveness of European building codes in ensuring a suitable seismic behaviour for RC bridges exposed to corrosive environments (henceforth referred to as the compliant bridge).
- A concrete cover of 20 mm was also considered to estimate the detrimental effects on the capacity of RC bridges exposed to corrosive environments in the case of non-compliant structural details such as a gross error during construction (henceforth referred to as the non-compliant bridge).

When assessing the capacity of the RC bridge affected by corrosion phenomena, a null initial concentration of chlorides was considered and the initial values of temperature and pore relative humidity were taken as 296.15 K and 0.65, respectively. A total surface chloride content equal to 7 kg/m^3 of concrete was assumed, which is representative of exposure conditions close to the Mediterranean coast (Val, 2004). Temperature (K) and relative humidity on the boundary were taken to vary with time (t in days) according to:

Table 1. Static loads on the RC bridge

Load type	Load: kN/m	Load: kN
Dead load	200.0	—
Live load (lumped, vehicles)	—	1200.0
Live load (distributed)	54.5	—

15. $$\tau = 296.15 - 15\sin(2\pi t/365)$$

16. $$h = 0.65 + 0.15\sin(\pi t/365)$$

A high pitting factor ($R = 8$) was considered, following the assumption of loss of rebar cross-section dominated by pitting corrosion. The following assumptions were also adopted for the sake of simplicity: (*a*) corrosion affects only the bridge columns; corrosion of the bridge deck and abutments is not considered; (*b*) spatial variability of chloride penetration is neglected.

4.2 Seismic input

Non-linear dynamic and static analyses were performed to estimate the seismic transverse response of the bridge. A set of seven ground motion (GM) records was selected by taking into account the design response spectrum as a target in order to perform IDA, which was used for a comparative evaluation of IMPAβ. Spectral matching for the range of relevant periods was the criterion adopted to define the set of GM records. The program Rexel (Iervolino *et al.*, 2010) was thus employed to extract seven unscaled GM records compatible, on average, with the target spectrum. The periods of the first three transversal modes of vibrations of the bridge are 0.649 s, 0.526 s and 0.125 s. The corresponding participating mass ratio values are 16.94%, 71.33% and 4.53%, respectively. A very small difference was found between the modal properties of the uncorroded and corroded bridge, in agreement with the results reported elsewhere (Alipour *et al.*, 2011) for RC bridges with a similar span length. The selected GM records are listed in Table 2 and the elastic acceleration spectral values S_a (with damping ratio equal to 5%) are given in Figure 5 for periods up to 4 s.

4.3 Numerical modelling

The capacity of uncorroded and corroded bridge columns was evaluated within the open-source framework OpenSees (Mazzoni *et al.*, 2006) . The cross-section was discretised using Q10 uniaxial fibres under the hypotheses of plain sections. In agreement with the work of Alipour *et al.* (2013), the simplifying assumption of a perfect steel–concrete bond was also adopted. The uniaxial material model Concrete01 available in OpenSees

Table 2. List of the selected GM records (note that RS5 and RS6 are two aftershock records)

Label	Earthquake name	Waveform	Date	PGA: *g*
RS1	South Iceland	4674-xa	17 June 2000	0.31
RS2	South Iceland	4674-ya	17 June 2000	0.31
RS3	Bingol	7142-xa	1 May 2003	0.50
RS4	Bingol	7142-ya	1 May 2003	0.50
RS5	South Iceland (aftershock)	6349-xa	21 June 2000	0.72
RS6	South Iceland (aftershock)	6332-ya	21 June 2000	0.51
RS7	South Iceland	6277-ya	17 June 2000	0.35
Average		—	—	0.46

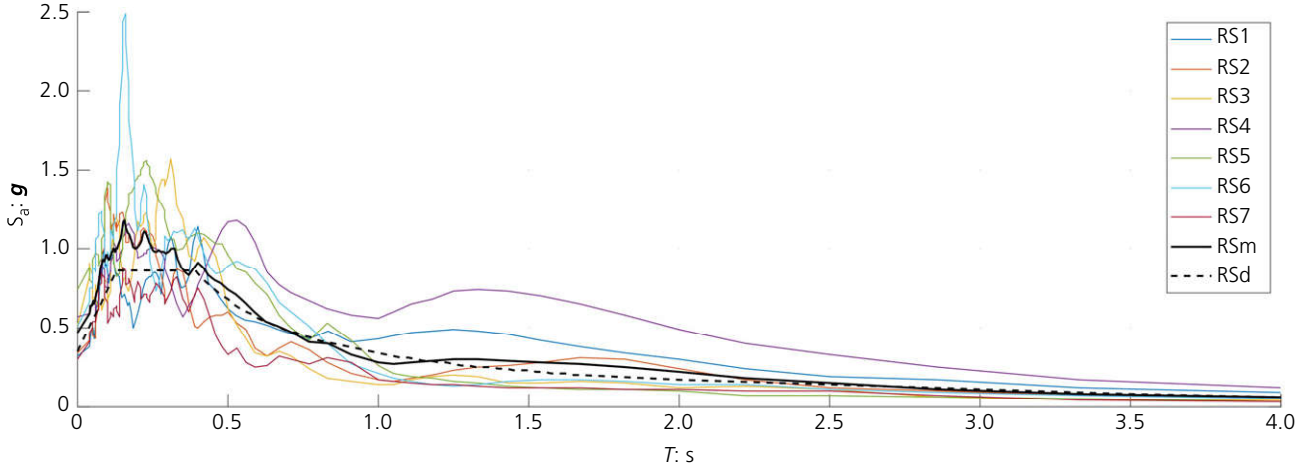

Figure 5. Elastic unscaled acceleration response spectra (RS1–RS7) of the selected seven GM records (damping ratio of 5%), corresponding median response spectrum (RSm) and design response spectrum (RSd)

was used to simulate the behaviour of both the core and cover concrete fibres. This model implements the Kent–Scott–Park concrete model with linear softening post-peak behaviour under compression and zero tensile strength in tension. To account for the spiral confinement, the concrete compressive strength, concrete strain at maximum strength and concrete strain at crushing were evaluated following Mander *et al.* (1998). The effect of corrosion on the core concrete confinement was considered by adopting the current corroded cross-sectional area of the spiral. The modified Monti–Nuti uniaxial material model (named SteelMN) was used to simulate the inelastic behaviour of rebars in tension and compression for both the corroded and uncorroded cases. It is noted here that SteelMN is not a material model available in OpenSees, but was developed in house from a series of previous studies (Lavorato *et al.*, 2019; Zhou *et al.*, 2015). The model defines an envelope skeleton curve constituted of straight segments – with elastic and plastic branches characterised by the elastic modulus E and the hardening ratio b – that intersect at the yielding (ε_{yn}, f_{yn}) and inversion (ε_{rn-1}, f_{rn-1}) point, respectively. The model is characterised by isotropic and kinematic hardening, and includes appropriate updating rules for E, b and R_s, where R_s is the parameter that governs the transition from the elastic to the inelastic branch. Additionally, the model is able to account for bar buckling in compression (in this case, b takes a negative value).

Some of the major characteristics of the model are shown in Figure 6. In the current version, SteelMN does not limit the maximum deformation automatically; thus the MinMax uniaxial material model available in OpenSees was associated to it in order to account for the reduced ultimate strain of the rebars due to pitting corrosion.

Pacific Earthquake Engineering Research Center guidelines (Aviram *et al.*, 2008) were adopted to simulate the main properties of the bridge in the numerical FE model (i.e. mass distribution, strength, stiffness and deformability of the bridge). The FE-based program SAP2000 (CSI, 2021) was employed for structural analysis of the bridge. In detail, 3D frame elements were adopted to model the columns and girders supporting the deck. The box girder was defined using the SAP2000 section designer. Rigid links in the transversal direction were used to model the connections between the superstructure and abutments. The lumped plasticity model was adopted for the columns; that is, the column elements were modelled assuming a plastic hinge where large plastic deformations were expected. The plastic hinges were modelled by means of SAP2000 fibre (P-M2-M3) hinges. The length of the plastic hinges was defined according to the work of Ou and Nguyen (2014). A reduced plastic hinge length was considered for the corroded columns. Specifically, the length of the corroded column plastic hinge was calibrated proportionally to the corrosion level, with average normalised hinge lengths of 0.98, 0.96, 0.88 and 0.80 adopted for corrosion levels of 10%, 15%, 20% and 25%, respectively (linear interpolation was used for intermediate levels of corrosion). Following Lavorato *et al.* (2019), it was confirmed that the spiral confinement was effective in preventing inelastic rebar buckling under compression for both the corroded and uncorroded bridge columns. The monitoring point was placed at the midspan of the deck.

Finally, the non-linear time-dependent partial differential equations governing chloride penetration into concrete were solved by means of the FE method using Comsol Multiphysics (Comsol Inc., 2021). To this end, a time step equal to 1 day

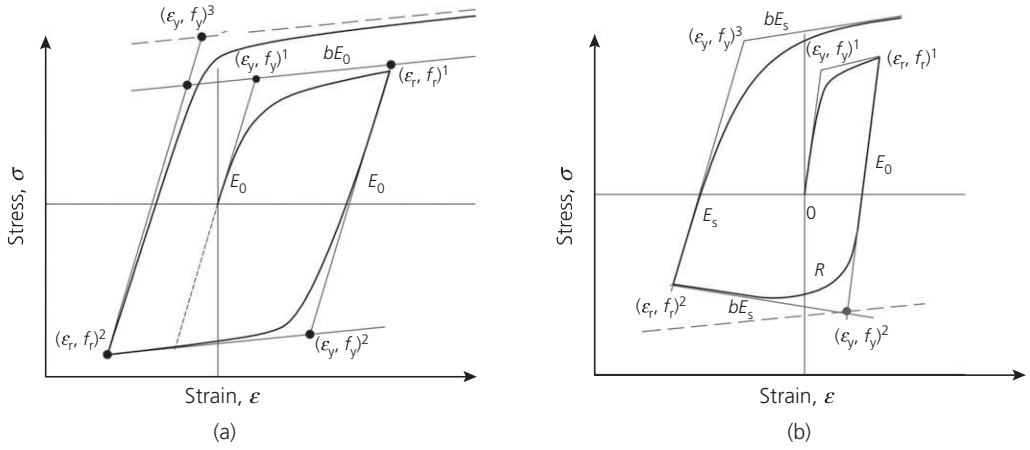

Q24 Q23 **Figure 6.** Main features of the implemented steel reinforcement model: (a) without bar buckling; (b) with bar buckling in compression

was considered together with a standard solver based on the Newton–Raphson method.

4.4 Results and discussion

The time-dependent loss of cross-sectional areas for the transverse and longitudinal reinforcements is detailed in Figure 7 and Table 3. As expected, the effects of corrosion were more evident for the transverse reinforcement due to the smaller distance from the boundary exposed to chlorides and also because the loss of cross-sectional area for small-diameter rebars is larger than for large-diameter rebars. The analysis for the corroded bridge was performed at $t = 75$ years.

The relationship between curvature (χ) and bending moment (M) for two RC bridge columns is shown in Figure 8 – it is evident that corrosion had a significant impact on the global non-linear behaviour of the columns. Figure 9 provides a comparison of the results obtained from IMPAβ and IDA for the uncorroded and corroded bridge. The non-compliant bridge ($c = 20$ mm) was considered to evaluate the differences between the two methods when the effects of corrosion were more evident. In general, the capacity curves (u_r–V_b) obtained by means of the two methods were similar (Figure 9(a)). The maximum values of V_b obtained from IMPAβ and IDA were almost the same. Furthermore, IMPAβ and IDA predicted a similar reduction in the maximum value of V_b due to corrosion. On the other hand, IMPAβ led to a lower estimation of the maximum value of u_r than IDA for both the uncorroded and corroded bridge.

Analysis of the incremental curves (u_r–PGA) obtained by means of the two methods provides further useful information in this regard (Figure 9(b)). The values of u_r predicted by IMPAβ and IDA were almost the same up to a seismic intensity level equal to the design PGA, whereas rather significant differences were obtained above this threshold. It should be recalled, however, that IDA is also influenced to some extent by the scaling procedure of the seismic records (Zacharenaki *et al.*, 2014) when the scale factor is higher than 1 (which corresponds to the design situation). This, in turn, also introduces a bias in the comparison between IMPAβ and IDA. Overall, Q11

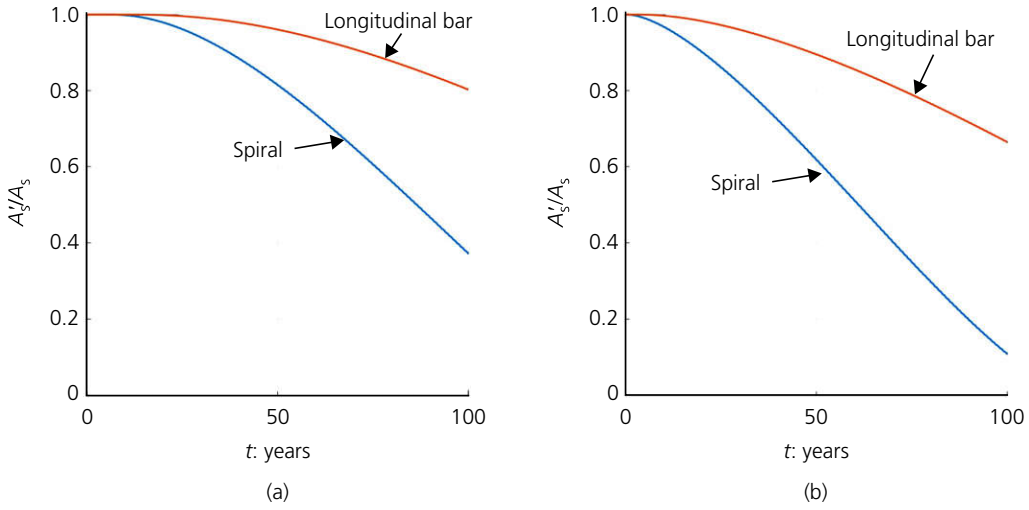

Figure 7. Time-dependent evolution of cross-sectional area ratio (A_s'/A_s) for transverse and longitudinal reinforcement under chloride-induced corrosion: (a) $c = 50$ mm; (b) $c = 20$ mm

Table 3. Time-dependent evolution of cross-sectional area ratio (A_s'/A_s) for different periods of exposure

Concrete cover thickness, c: mm		A_s'/A_s: %				
		0	25 years	50 years	75 years	100 years
50	Longitudinal bar	100.0	99.6	96.0	89.3	80.2
50	Spiral	100.0	96.1	81.5	60.5	37.1
20	Longitudinal bar	100.0	97.2	89.5	78.9	66.4
20	Spiral	100.0	86.1	61.8	34.8	10.8

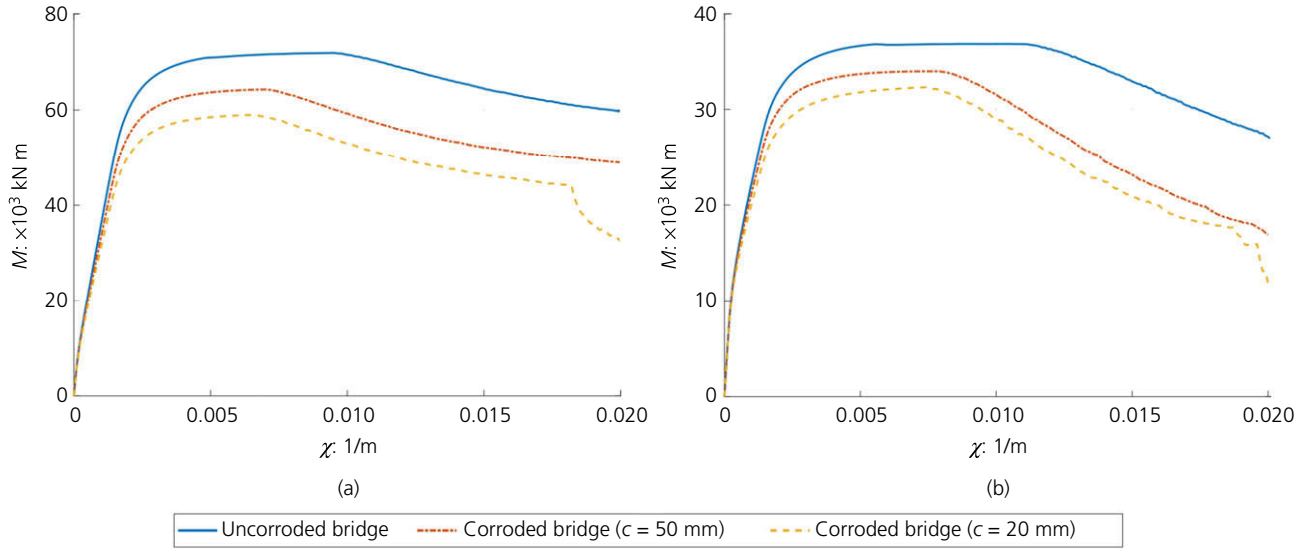

Figure 8. Curvature–moment responses: (a) shortest column; (b) tallest column. The results for the corroded bridge refer to $t = 75$ years

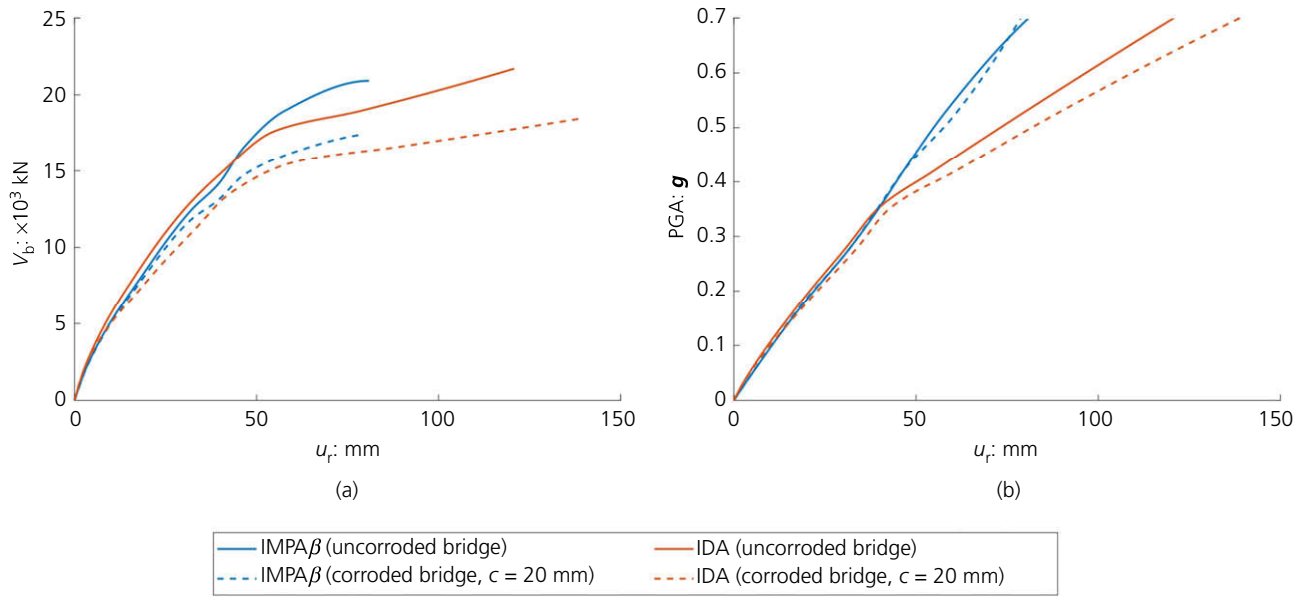

Figure 9. Comparison of IMPAβ and IDA for the uncorroded and corroded RC bridge: (a) capacity curves u_r–V_b; (b) incremental curves u_r–PGA. The results for the corroded bridge refer to $t = 75$ years

taking into account the large reduction in modelling and computational efforts, these results demonstrate that IMPAβ is in satisfactory agreement with IDA and can be considered a suitable alternative tool for the analysis of corroded RC bridges, especially in view of the fact that this might be required at several points in time.

Figure 10 shows the bridge response obtained by means of IMPAβ (i.e. transverse displacements of the deck when the monitoring point achieved the PP for each seismic intensity were considered in the analysis). The figure shows comparisons the deformed shapes of the uncorroded and corroded bridge (both compliant and non-compliant bridges were considered in

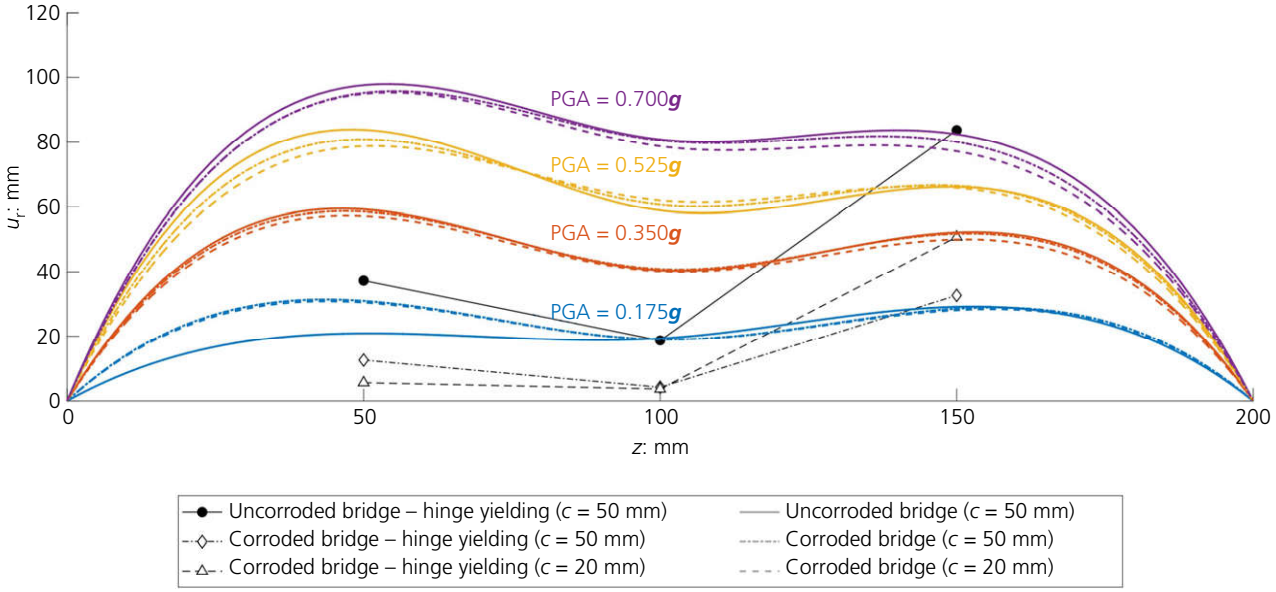

Figure 10. Deformed shapes for uncorroded and corroded RC bridge for different PGAs. The results for the corroded bridge refer to $t = 75$ years

the case of corrosion). The deformed shape was constructed by fitting the displacement values calculated at the controlled joints (i.e. deck joints at the position of the piers). The median response from the response spectra of the selected seismic GMs was assumed to define a single PP.

Figure 10 shows that the deformed shapes were characterised by displacements oriented along the same direction. Furthermore, the figure highlights that deck deformation at pier 1 is worthy of special consideration in view of its influence on the global non-linear behaviour of the structure. It is evident that the displacements experienced by the corroded bridge were higher than those occurring in the uncorroded bridge for low seismic intensity levels up to PGA = 0.175***g***. For higher intensity levels (i.e. PGAs of 0.525***g*** and 0.700***g***), the transverse displacement of the deck under corrosion was less than that estimated for the uncorroded bridge. Plastic hinge activation is decisive for explaining this counter-intuitive evidence due to the global non-linear behaviour. In fact, in order to evaluate the PP according to the capacity spectrum method, the elastic-to-dissipated energy ratio plays a crucial role and it rules the different non-linear behaviours of the uncorroded and corroded bridge. For high-intensity seismic actions (i.e. PGAs of 0.525***g*** and 0.700***g***), pier 3 behaved elastically for the uncorroded bridge and thus the elastic energy scaled up with the deformation. In the case of the corroded bridge, all the hinges yielded and hence the dissipated energy had a more relevant effect on reducing the performance in terms of displacements. For a lower seismic intensity level (i.e. PGA = 0.175***g***), the response of pier 3 was still within the elastic range and a plastic hinge occurred at pier 2 regardless of the bridge condition, whereas a plastic hinge was only activated at pier 1 if it was affected by corrosion. It is interesting to note that, while plastic hinges occurred at the shorter piers (i.e. piers 1 and 2) almost immediately under corrosion whatever the concrete cover thickness, a plastic hinge occurred at the longest pier (pier 3) under corrosion at the design PGA value if the concrete cover complied with the standards and at half such a value (i.e. for PGA = 0.175***g***) otherwise.

Altogether, these results indicate that the effects of corrosion phenomena on the RC bridge were mainly reflected in the ductility demand, and design provisions regarding structural durability can have a significant impact on the expected seismic behaviour. The consequences of corrosion phenomena on the ductility demand of the corroded RC bridge can be better inferred from Figure 11, where u_y and u_u are the yielding displacement and ultimate displacement calculated according to Fema 356. Q12

Analysis of the capacity curves (u_r–V_b) reveals that the maximum values of V_b for the compliant and non-compliant corroded RC bridge were, respectively, about −12% and −17% of those for the uncorroded bridge, thereby resulting a rather modest reduction after a quite long time period. Conversely, a much larger corrosion effect was observed in terms of the required ductility. For the design PGA, u_r/u_y for the compliant corroded bridge was about 43% greater than that for the

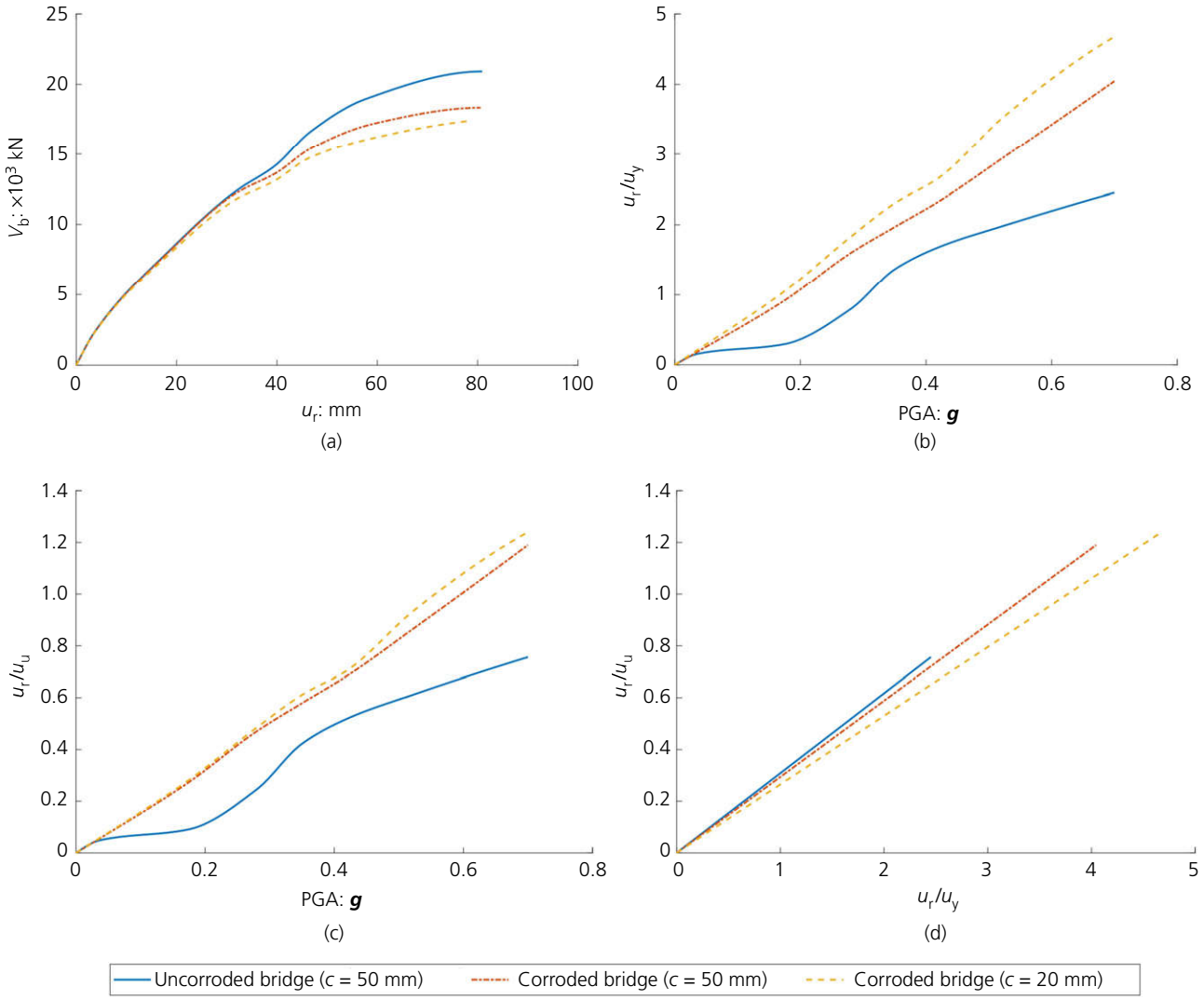

Figure 11. Outcomes for uncorroded and corroded RC bridge ($t = 75$ years): (a) capacity curves u_r–V_b; (b) ductility demand curves u_r/u_y–PGA; (c) ultimate capacity ratio curves u_r/u_u–PGA; (d) relationship between ductility demand u_r/u_y and ultimate capacity ratio u_r/u_u

uncorroded bridge, with this value increasing to 67% if the concrete cover was not compliant with the standards. The higher the PGA, the larger were the effects of corrosion on the required ductility. For example, for PGA = 0.700***g***, u_r/u_y values for the compliant and non-compliant corroded bridge were about 65% and 89% greater than the values for the uncorroded bridge. The results in terms of u_r/u_u align with those for u_r/u_y obtained for the compliant corroded RC bridge, but regardless of the concrete cover thickness. In fact, u_r/u_u values for the (compliant or non-compliant) corroded bridge were found to be about 36% and 57% greater that the values for the uncorroded bridge for the same PGA. It seems that compliant or non-compliant realisation of the concrete cover has large effect on u_r/u_y and negligible consequences on u_r/u_u. This, however, might depend on the epistemic uncertainties associated with the definition of the yielding point. Figure 11 also highlights that the uncorroded bridge was able to withstand seismic intensity levels higher than those relevant for the design stage within the limits of the considered ductility level, but this did not hold true for the corroded case (recall that a behaviour factor of $q = 3.0$ was assumed).

5. Conclusions

Seismic assessments of corroded RC bridges must cope with two important but conflicting needs. On the one hand, structural analysis and corrosion evaluation requires the development of rather sophisticated numerical models. On the other, the use of such tools can result in a large increase in modelling

effort and elaboration time, which might be prohibitive for ordinary bridge structures. Motivated by this evidence, a simplified – yet accurate – computational framework for the seismic analysis of RC bridges under chloride-induced corrosion was developed in this study. The main findings of this study are summarised as follows.

- IMPA for bridges (IMPAβ) compares satisfactorily with IDA even in the case of severe corrosion phenomena. The maximum base shear values obtained by the two methods were very similar, as was the corresponding predicted reduction due to corrosion. However, the two methods differed in predictions of deck displacements for seismic intensity levels greater than the design condition. Taking into account the simplification associated with a non-linear static procedure with respect to a dynamic one, it can be concluded that IMPAβ is a valid alternative tool for the seismic assessment of corroded RC bridges.
- Long-term performance forecasting of RC bridges under pitting corrosion calls for a multi-physics analysis, but some simplifications can be introduced in the numerical model of chloride ingress to alleviate the computational burden. A combination of physics-based models to account for the effects of temperature, humidity and aging together with data-driven modelling to simulate the effect of concrete cover cracking due to rebar corrosion is a viable strategy to prevent a dramatically increment of the computational burden.
- In-depth analysis of a practical case study demonstrated that, if an irregular RC bridge with severe pitting-induced corrosion on its columns has been designed in compliance with modern standards, then the long-term reduction in capacity in terms of base shear is rather limited. However, a large increment in the required ductility is observed, which must thus be considered as the most critical issue. In this regard, an irregular bridge layout and non-compliant realisation of the concrete cover also deserve proper attention as they influence the occurrence of plastic hinges.

Acknowledgements

The authors acknowledge the funding received by ReLUIS – Laboratories University Network of seismic engineering (research project ReLUIS/DPC 2019–2021) and the National Natural Science Foundation of China (grant agreement 51778148). The work of Giuseppe Quaranta is framed within the research project 'Smart technologies and decision support tools for the assessment of deteriorating reinforced concrete infrastructures in seismic areas at territorial scale' (grant RM120172B37F0628), funded by Sapienza University of Rome.

REFERENCES

Afsar DE (2021) Modelling strategy impact on structural assessment of deteriorated concrete bridge columns. *Proceedings of the Institution of Civil Engineers – Bridge Engineering* https://doi.org/10.1680/jbren.21.00003. Q13 Q14

Afsar DE and Kashani MM (2021) Nonlinear structural performance and seismic fragility of corroded reinforced concrete structures: modelling guidelines. *European Journal of Environmental and Civil Engineering* https://doi.org/10.1080/19648189.2021.1896582. Q15 Q16

Alipour A, Shafei B and Shinozuka M (2011) Performance evaluation of deteriorating highway bridges located in high seismic areas. *Journal of Bridge Engineering* **16(5)**: 597–611.

Alipour A, Shafei B and Shinozuka MS (2013) Capacity loss evaluation of reinforced concrete bridges located in extreme chloride-laden environments. *Structure and Infrastructure Engineering* **9(1)**: 8–27.

Andisheh K, Scott A and Palermo A (2016) Seismic behavior of corroded RC bridges: Review and research gaps. *International Journal of Corrosion* **2016**: 3075184, https://doi.org/10.1155/2016/3075184.

Aviram A, Mackie KR and Stojadinović B (2008) *Guidelines for Non-Linear Analysis of Bridge Structures in California*. Pacific Earthquake Engineering Research Center, Berkeley, CA, USA.

Bergami AV, Liu X and Nuti C (2015) Proposal and application of the incremental modal pushover analysis (IMPA). *Proceedings of IABSE Conference–Structural Engineering: Providing Solutions to Global Challenges*. Q17

Bergami AV, Forte A, Lavorato D and Nuti C (2017) Proposal of a incremental modal pushover analysis (IMPA). *Earthquakes and Structures* **13(6)**: 539–549.

Bergami AV, Fiorentino G, Lavorato D, Briseghella B and Nuti C (2020a) Application of the incremental modal pushover analysis to bridges subjected to near-fault ground motions. *Applied Sciences* **10(19)**: 6738.

Bergami AV, Nuti C, Lavorato D, Fiorentino G and Briseghella B (2020b) IMPAβ: incremental modal pushover analysis for bridges. *Applied Sciences* **10(12)**: 4287.

BSI (2011) BS EN 1998-2:2005/A2:2011: Eurocode 8: Design of structures for earthquake resistance. Bridges. BSI, London, UK.

BSI (2013) BS EN 1998-1:2004/A1:2013: Eurocode 8: Design of structures for earthquake resistance. General rules, seismic actions and rules for buildings. BSI, London, UK.

Comsol Inc. (2021) *COMSOL Multiphysics Version 5.3*. Comsol Inc., Stockholm, Sweden. See https://uk.comsol.com/release/5.3 (accessed 10/11/2021).

Conti E, Malerba PG, Quagliaroli M and Scaperrotta D (2020) Residual capacity of a reinforced concrete grillage deck exposed to corrosion. *Structure and Infrastructure Engineering* **16(1)**: 202–218.

Coronelli D and Gambarova P (2004) Structural assessment of corroded reinforced concrete beams: modeling guidelines. *Journal of Structural Engineering* **130(8)**: 1214–1224.

CSI (Computers and Structures, Inc.) (2021) *SAP2000 Nonlinear Version 10*. CSI, Walnut Creek, FL, USA. See https://www.csiamerica.com/products/sap2000 (accessed 10/11/2021).

Dizaj EA and Kashani MM (2020) Numerical investigation of the influence of cross-sectional shape and corrosion damage on failure mechanisms of RC bridge piers under earthquake loading. *Bulletin of Earthquake Engineering* **18**: 4939–4961, https://doi.org/10.1007/s10518-020-00883-3.

Iervolino I, Galasso C and Cosenza E (2010) REXEL: computer aided record selection for code-based seismic structural analysis. *Bulletin of Earthquake Engineering* **8(2)**: 339–362.

Imperatore S, Rinaldi Z and Drago C (2017) Degradation relationships for the mechanical properties of corroded steel rebars. *Construction and Building Materials* **148**: 219–230. Q18

Kashani M, Maddocks J and Dizaj EA (2019) Residual capacity of corroded reinforced concrete bridge components: a state of the art review. *Journal of Bridge Engineering* **24(7)**: 1–16.

Kwon SJ, Na UJ, Park SS and Jung SH (2009) Service life prediction of concrete wharves with early-aged crack: probabilistic approach for chloride diffusion. *Structural Safety* **31(1)**: 75–83.

Lavorato D, Fiorentino G, Pelle A *et al.* (2019) A corrosion model for the interpretation of cyclic behavior of reinforced concrete sections. *Structural Concrete* **21(5)**: 1732–1746.

Liu T and Weyers RW (1998) Modeling the dynamic corrosion process in chloride contaminated concrete structures. *Cement and Concrete Research* **28(3)**: 365–379.

Liu Y (1996) *Modeling the Time-to Corrosion Cracking of the Cover Concrete in Chloride Contaminated Reinforced Concrete Structures*. PhD thesis, Virginia Tech, Blacksburg, VA, USA.

Mander JB, Priestley MJN and Park R (1998) Theoretical stress-strain model for confined concrete. *Journal of Structural Engineering* **114(8)**: 1804–1826.

Mazzoni S, McKenna F, Scott MH and Fenves GL (2006) *OpenSEES Command Language Manual*. Pacific Earthquake Engineering Research Center, Berkeley, CA, USA.

MDIT (Ministero Delle Infrastrutture e dei Trasporti) (2018) Decreto 17 gennaio 2018 «Aggiornamento delle Norme tecniche per le costruzioni». GU Serie Generale n.42 del 20-02-2018 – Suppl. Ordinario n. 8. Rome, Rome, Italy (in Italian).

Ou YC and Nguyen ND (2014) Plastic hinge length of corroded reinforced concrete beams. *ACI Structural Journal* **111(5)**: 1049–1058.

Pang Y, Wei K and Yuan W (2020) Life-cycle seismic resilience assessment of highway bridges with fiber-reinforced concrete piers in the corrosive environment. *Engineering Structures* **222**: 111120.

Shafei B, Alipour A and Shinozuka M (2012) Prediction of corrosion initiation in reinforced concrete members subjected to environmental stressors: a finite-element framework. *Cement and Concrete Research* **42(2)**: 365–376.

Shafei B, Alipour A and Shinozuka M (2013) A stochastic computational framework to investigate the initial stage of corrosion in reinforced concrete superstructures. *Computer-Aided Civil and Infrastructure Engineering* **28(7)**: 482–494.

Val DV (2004) *Aspects of Corrosion in Reinforced Concrete Structures and its Influence on Structural Safety*. National Building Research Institute, Report 2002950.

Val DV (2007) Deterioration of strength of RC beams due to corrosion and its influence on beam reliability. *Journal of Structural Engineering* **133(9)**: 1297–1306.

Vidal T, Castel A and Francois R (2004) Analyzing crack width to predict corrosion in reinforced concrete. *Cement and Concrete Research* **34(1)**: 165–174.

Zacharenaki A, Fragiadakis M, Assimaki D and Papadrakakis M (2014) Bias assessment in incremental dynamic analysis due to record scaling. *Soil Dynamics and Earthquake Engineering* **67**: 158–168.

Zhang SF, Lu CH and Lui RG (2011) Experimental determination of chloride penetration in cracked concrete beams. *Procedia Engineering* **24**: 380–384.

Zhou X, Tu X, Chen A and Wang Y (2019) Numerical simulation approach for structural capacity of corroded reinforced concrete bridge. *Advances in Concrete Construction* **7(1)**: 11–22.

Zhou Z, Lavorato D, Nuti C and Marano GC (2015) A model for carbon and stainless steel reinforcing bars including inelastic buckling for evaluation of capacity of existing structures. *Proceedings of the 5th ECCOMAS Thematic Conference on Computational Methods in Structural Dynamics and Earthquake Engineering, Crete*, pp. 25–27.